Acta Astronautica 197 (2022) 35–45

Contents lists available at ScienceDirect

Acta Astronautica

journal homepage: www.elsevier.com/locate/actaastro

Research paper

Optimal design of tube flexure cut-out geometries for deployment performance

Pathawee Kunakorn-ong, Zahra Soltani, Matthew Santer *

Department of Aeronautics, Imperial College London, London SW7 2AZ, UK

ARTICLE INFO

Keywords:
Tube flexure
Deployable structure
Bayesian optimization

ABSTRACT

A design methodology is proposed for deployable tube flexures made of ultra-thin carbon fiber composite. The methodology is developed to achieve desired stowage and deployment performance in the absence of material failure. The cut-out shape in the tube flexure is determined by means of a Bayesian optimization technique. The objective function is defined based on both desired moment characteristics and Hashin failure criteria. Multiple cut-out parameterization schemes are presented. Bayesian optimization is shown to be effective and significant performance improvements are achieved thought use of spline-based optimization in comparison to more conventional forms. The efficiency of the approach is validated via experiment.

1. Introduction

Deployable structures are of considerable interest in the space industry because they enable large structures with operational dimensions greater than existing launcher fairings. For large space structures such as solar sails, antennas, and synthetic aperture radars, these structures are first fabricated on the ground and then packed into a small configuration for stowage and transportation to space. When the structure arrives at its desired location, it is expanded into its operational configuration.

Compliant flexures are one kind of deployable structure used to connect two or more structural members replacing conventional mechanical hinges. The flexures considered in this paper are fundamentally based on tape springs. Deployment and stowage of metallic tape springs have been studied in great detail [1]. They exhibit a nonlinear relationship between moment and rotation for a nonlinear elastic fold of the spring which is dependent on the directions of applied end moment and curvature of its cross-section. The behavior of metallic tape springs is well understood [2,3]. The trend in recent research has been towards the use of fiber reinforced polymers because of its tailorable material properties [4] and the application of parallel tape springs to form tube flexures [5,6]. These are typically manufactured by cutting slits out of thin-walled tube structures.

This paper considers the design of two parameterized cut-out geometries in deployable tube flexures. The motivation for this is inspired by a conventional dogbone shape cut-out presented in the tube flexure implementation on the MARSIS deployable antenna [7] that was launched in 2003. By introducing the cut-out geometries, the tube flexure is allowed to elastically fold and deploy. The cut-out geometries greatly affect the operational moments and stiffness of tube flexures. However, the dogbone geometry significantly constrains the design space and consequently the achievable performance. In this work, therefore, multiple cut-out parameterization schemes are determined and optimized for deployment performance and resilience to failure. It is noted that the global flexure dimensions, materials, and layups may additionally be design variables. However, in this paper, we have specifically focused on the optimization of the cut-out geometries to achieve a desired moment performance. The rationale behind this decision is that these additional parameters are largely fixed by other systems-level requirements.

Design optimization has been previously been integrated into the design of deployable structures to optimize for specific operational requirements. For example, the shape optimization of deployable reflectors with an edge stiffener was presented in [8]. The Response Surface Methodology (RSM) was employed to optimize the stiffness of tape springs using fitted quadratic response polynomial function [9]. In a similar approach, RSM is applied for parametric study and the Modified Non-Dominated Sorting Genetic Algorithm (NSGA-II) was used to optimize the rectangular cut-out with rounded ends and the stiffness of tube flexures [10]. The parametric optimization of composite tube flexures has been studied to optimize the slot geometry in terms of the length, width, and circle of slot ends [11].

However, previous studies were limited to the conventional cut-out geometry with a longitudinal rectangle and rounded or circular ends. Furthermore, the behavior of deployable structures presents a

* Corresponding author.
E-mail address: m.santer@imperial.ac.uk (M. Santer).

https://doi.org/10.1016/j.actaastro.2022.04.034
Received 10 February 2022; Received in revised form 9 April 2022; Accepted 28 April 2022
Available online 6 May 2022
0094-5765/© 2022 The Author(s). Published by Elsevier Ltd on behalf of IAA. This is an open access article under the CC BY-NC-ND license (http://creativecommons.org/licenses/by-nc-nd/4.0/).

highly nonlinear response in both geometry and material. Therefore, in this paper, a robust design methodology for deployable tube flexures is proposed using a generalized cut-out parameterization and derivative-free Bayesian optimization, where Bayesian optimization is a class of machine-learning-based optimization and suitable for solving expensive-to-evaluate functions [12].

The present paper proposes two methodologies for the design of deployable tube flexures for deployment performance and resistance to failure. Bayesian optimization is employed to optimize conventional and spline-based cut-out geometries based on an established objective function. Bayesian optimization is shown to be effective and significant improvement on moment performance whilst retaining failure tolerance is achieved using spline-based parameterization compared to conventional cut-out geometry. Finally the methodology is validated experimentally.

2. Optimization methodology

In this section, the design optimization methodology is presented. The design process aims to optimize cut-out geometries in a tube flexure using Bayesian optimization. A numerical simulation of the tube flexure model is presented to simulate the folding process.

In this paper, we consider a composite tube flexure with a 30 mm diameter and 140 mm length, similar to the MARSIS segment sizing [7], with two identical longitudinal cut-outs. The rectangle–circle cut-out, or conventional geometry, is considered as a baseline used to assess the effectiveness of the novel spline-based parameterization, referred from the literature [7,11]. Based on previous studies [7,10,11], the cut-out shape is limited to a simple geometry which is a rectangle with circular or rounded ends. A problem associated with this cut-out geometry is that strain is highly localized near the circular edges and in the transition region between the rectangle and the circular ends [11], so that these areas have a tendency to fail during the folding, consequently causing a deployment malfunction. Hence, in this current work, a spline-based parameterization is proposed to tackle that limitation. The spline parameters allow the design points to form a wide range of cut-out shape within the design space providing the flexibility to avoid stress concentration.

2.1. Optimization process

The optimization process proposed in this research is summarized in the flowchart in Fig. 1. First, design parameters are defined for two types of rectangle–circle and spline cut-outs. The objective function is formulated from operational moment–rotation behavior including maximizing peak moment, achieving a desired value of post-buckle moment, and avoiding material failure during folding. Bayesian optimization implemented in this paper is a derivative-free method to optimize nonlinear problems disregarding gradient-based which is suitable to solve nonlinear moment–rotation behavior and material failure of deployable tube flexure. The initial data collection is prepared randomly. Then, a surrogate model of objective function is performed using the 'Regression Learner' implemented in MATLAB [13] with optimized hyperparameters. This step provides a Bayesian posterior probability distribution of the objective function based on an available data collection. Next, Bayesian optimization 'bayesopt' [13] is employed to calculate an acquisition function using the current posterior distribution. The acquisition function will determine the next sampling point balancing between objective improvement and unexplored design space. The next result is added to the current data collection and the posterior distribution is then updated to continue the next optimization loop. The feasible designs are obtained when the peak moment is greater that the target without material failure. Finally, the optimization is terminated when a moving average of absolute error of candidate point obtained from Bayesian and FE results is lower than 10% to justify the convergence, and the tube performance meets with the objective requirements.

2.2. Finite element modeling

The cut-outs are superimposed on the surface of the tube. The folding simulation is then carried out by using the finite element method employing the ABAQUS/Explicit commercial solver [14]. In order to simulate the folding condition, rotation is applied to representative nodes (shown as Point 1 and Point 2) at the centroid of the flexure cross section as shown in Fig. 2. The representative nodes are generated using multi-point constraints (MPC) for circumferential nodes on the ends of the tube. Point 1 is rotated about the x-axis by a 90° rotation while the translations and rotations on other degree of freedom are constrained. Point 2 is permitted to translate along the z-axis and rotates about x-axis by -90°, with all other degrees of freedom being restricted.

It should be noted that the folding simulation is carried out using displacement control for reasons of numerical stability. However, as will be shown in Section 3, a single moment–rotation response is required to generate the objective functions and therefore a folding condition of pure bending is required. Although this is not enforced by the simulation, a comparison of the reaction moments during folding at points 1 and 2 revealed that they were identical with the exception of a small region following initial snap though and that therefore a condition of pure bending may be assumed.

During the folding process, the surfaces of the tube come into self-contact after snap through at the middle of the tube and contact of the exterior walls occurs at fully folded configurations. The interaction of contact surfaces in the FE model is defined using General Contact [14]. This contact type was chosen to automatically specify the contact for the entire model and a frictionless condition is assumed.

The tube is modeled using 4-node shell elements with reduced integration (S4R). The element has 6 degrees of freedom per node i.e. translations along x, y and z directions and rotations about the nodal x, y and z axes. The tube model is partitioned to obtain uniform square elements at the middle part of the tube and the end regions. The tube flexure model consists of 6245 elements with a global element size of 1.25 mm. This level of discretization was confirmed to provide converged results for displacement and stress.

Additionally, the simulation of deployable structures involves highly nonlinear behavior including instability and dynamic snapping. To diminish artificial numerical effects, artificial damping can be applied as a viscous pressure load via ABAQUS/Explicit. This pressure damps nonphysical effects in the simulation. The viscous pressure is defined as

$$p = -c_v(\vec{v} \cdot \vec{n}) \tag{1}$$

where p is the applied pressure, c_v is the viscosity coefficient, $\vec{v}$ is the velocity of the point on the surface, and $\vec{n}$ is the unit outward normal of corresponding surface.

In a previous study [6], the application of artificial damping using the viscous pressure has been shown to be effective in reducing the noise in the simulation. Therefore, in this work a viscous pressure coefficient of $c_v = 5 \times 10^{-6} \rho c_d$ is adopted in which c_d is the dilatational wave speed.

In the next section, material properties used in the numerical simulation will be given. Two parameterized cut-out geometries are presented: the first is the conventional rectangular slot with circular ends inspired by the MARSIS deployable booms [7] and previous studies [11]; and the second is a spline-based geometry which allows a general formation of cut-out shape. An objective function is established associated with moment performance and material failure.

3. Model description for optimization

In this section, material properties of tube flexures are presented. The cut-out geometries are parameterized for rectangle–circle and spline cut-outs. An objective function is established as a user-defined function related to the operational characteristics of the tube flexures and Hashin failure criteria.

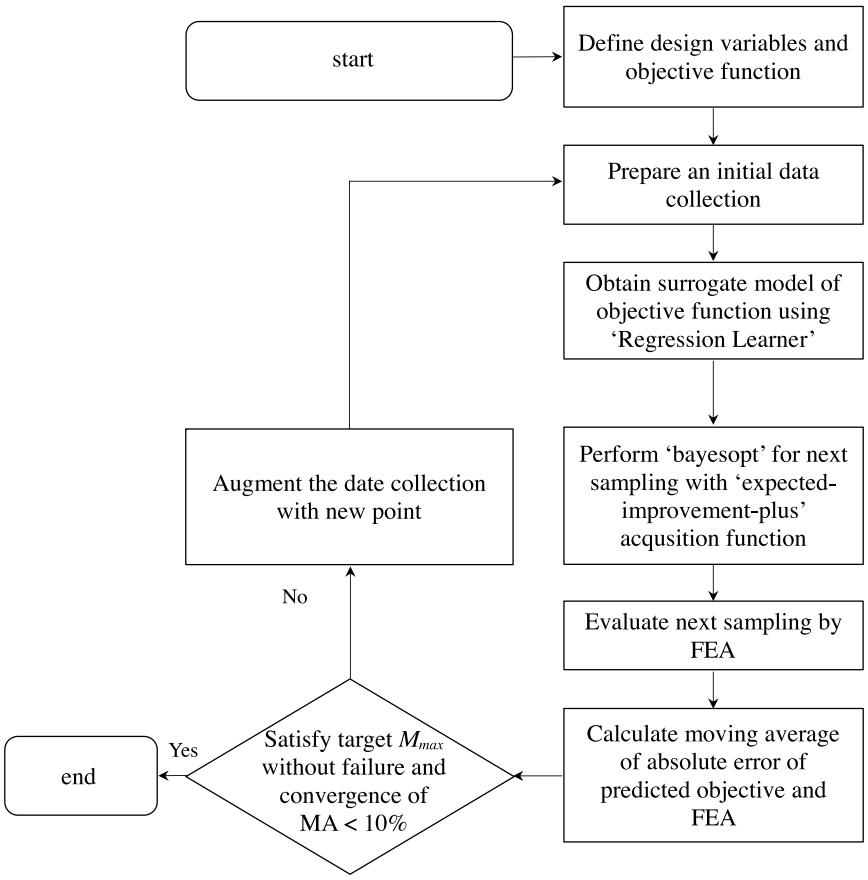

Fig. 1. Flowchart of the proposed optimization process.

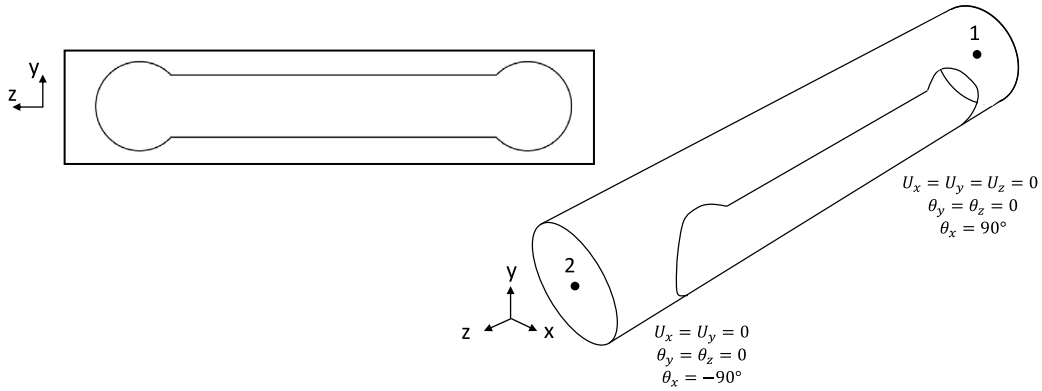

Fig. 2. Sketch of a tube flexure model with conventional cut-out highlighting the boundary conditions and applied rotation.

3.1. Material properties

The tube flexure is made of uni-directional pre-preg with Mitsubishi Pyrofil TR50S carbon fibers and a K51 Skyflex resin system. The tube flexure consists of a four-ply laminate $[-45°/45°]_2$ with a 20 μm thickness for each ply, where the principal material coordinate is along the cylinder axis. The material properties, as shown in Table 1, used in the Finite Element model were obtained from the material provider [15] and literature [16], where properties marked with an asterisk are estimated due to the unavailability of published data. The Hashin failure criteria [17] are implemented for failure prediction of unidirectional fiber composites, and damage evolution based on fracture energy, as shown in Table 2, is implemented to capture material softening. These material properties and failure criteria will be used in the numerical modeling section.

3.2. Geometry parameterizations

In this section, the design parameterizations for optimization are presented for rectangle–circle and spline cut-outs.

3.2.1. Rectangle-circle cut-out

The conventional cut-out geometry, Fig. 3(a), is parameterized by: the rectangle length, L, the rectangle width, d, the radius of end circle, r, and the offset distance between the end of rectangle and the center of circle, c. It should be noted that the parameterization illustrations

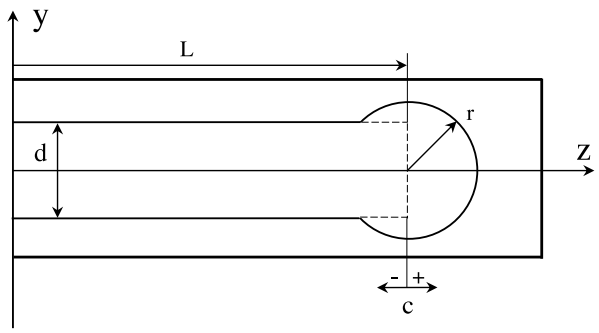

(a) Rectangle-circle geometry

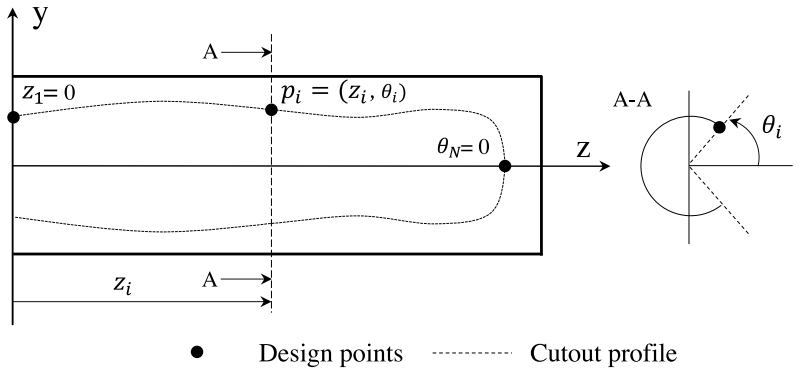

(b) Spline-based geometry

Fig. 3. Design parameters for cut-outs.

Table 1
Mechanical properties [15].

(Unit)	Values
Tensile modulus, E_1 (GPa)	125.3
Transverse modulus, E_2 (GPa)	8.4
Poisson's ratio (in-plane), ν_{12}	0.28
In-plane shear modulus, G_{12} (GPa)	5.1
Shear modulus in plane 1–3, G_{13} (GPa)	5.1
Shear modulus in plane 2–3, G_{23} (GPa)	2.8
Density, ρ (kg/m^3)	1596.8
Longitudinal tensile strength, F_{1t} (MPa)	2500
Longitudinal compressive strength, F_{1c} (MPa)	1200
Longitudinal shear strength, S_{12} (MPa)	175
Transverse tensile strength, F_{2t} (MPa)	120*
Transverse compressive strength, F_{2c} (MPa)	120*
Transverse shear strength, S_{21} (MPa)	120*

Table 2
Fracture energy [16].

Failure (kJ/m^2)	Values
Fiber tension	38.43
Fiber compression	25.1
Matrix tension	0.255
Matrix compression	1.662

presented in Fig. 3 show only the right-hand half of the flexure; the tubes are symmetrical about the $y-z$ plane. A negative value for the c parameter means the circle center is shifted to the $-z$ axis whereas a positive value means the circle center is shifted along the $+z$ axis, as illustrated in Fig. 3(a). The problem for optimizing the rectangle–circle cut-out can be defined as per Eq. (2) with the parameter bounded as shown

$$\begin{aligned} &\min && \textit{Objective} \\ &\text{s.t.} && 40\text{ mm} \le L \le 46\text{ mm} \\ &&& 8\text{ mm} \le d \le 11\text{ mm} \\ &&& 11\text{ mm} \le r \le 13\text{ mm} \\ &&& -3\text{ mm} \le c \le 1\text{ mm} \end{aligned} \tag{2}$$

3.2.2. Spline cut-out

The spline parameterization of the tube flexure is shown in Fig. 3(b), where the tube is symmetrical about the $y-z$ plane. Design points are defined as cylindrical coordinates, $p_i(z_i, \theta_i)$ for $i = 1, 2, 3, \ldots, N$, where N is the number of design points. z_i is an axial distance from the origin to a design point. θ_i is an angle between the -x axis to the design point while the radial distance is constant at 15 mm.

A cubic spline is used to connect the design points. The optimization of the spline cut-out is based on 5 control points, from which the cut-out profile can be defined by one quadrant and then using the symmetry planes to generate the entire profile. In order to maintain the shape of the cut-out, z_1 is equal to zero at the middle of tube flexure and θ_N is equal to zero to be the cut-out end. Additional constraints on z and θ are imposed to control the order of points and maintain the points within the design boundary of the tube. The optimization problems with variable constraints can be expressed as follows:

$$\begin{aligned} &\min_{z,\theta} && \textit{Objective} \\ &\text{s.t.} && z_i < z_{i+1} < 60\text{ mm} && i = 2, 3, 4, \ldots, N \\ &&& 10^\circ \le \theta_i \le 45^\circ && i = 1, 2, 3, \ldots, N-1 \end{aligned} \tag{3}$$

3.3. Definition of objective function

Operational characteristics of a tube flexure are introduced to define moment performance in the objective function. A typical moment–rotation diagram, as sketched in Fig. 4, presents the folding behavior of

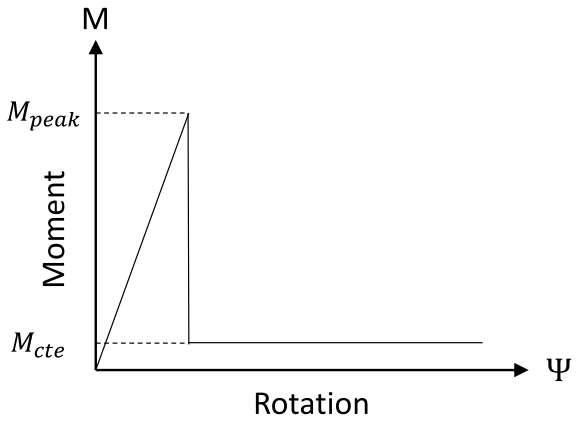

Fig. 4. Schematic moment–rotation diagram of a tube flexure used as the basis of the objective function.

the tube flexure under applied rotation. Initially, the moment increases linearly to the peak value M_{peak}. A higher value of M_{peak} indicates a tube flexure which is more resistant to buckling. After passing the limit point at M_{peak}, the moment drops to an approximately constant bending moment until the flexure is fully folded. In other words, this constant bending moment M_{cte} is a required moment to maintain the folding configuration in a package. The constant bending moment also defines the deployment behavior when the flexure is released so it is an important design objective. These two moments must be taken into account when developing the objective function.

Due to the use of unidirectional laminae, the Hashin criteria [17] are implemented to analytically predict the failure during folding. These criteria are used to predict the onset of material failure. The relevant material properties are shown in Tables 1–2. The four Hashin indices are incorporated to consider the in-plane failures: fiber failure in longitudinal direction (Eq. (4)), fiber failure in transverse direction (Eq. (5)), matrix failure in longitudinal direction (Eq. (6)), and matrix failure in transverse direction (Eq. (7)). The four Hashin indices are

$$f_{FT} = \left(\frac{\sigma_{11}}{F_{1t}}\right)^2 + \alpha\left(\frac{\tau_{12}}{S_{12}}\right)^2 \tag{4}$$

$$f_{FC} = \left(\frac{\sigma_{11}}{F_{1c}}\right)^2 \tag{5}$$

$$f_{MT} = \left(\frac{\sigma_{22}}{F_{2t}}\right)^2 + \left(\frac{\tau_{12}}{S_{12}}\right)^2 \tag{6}$$

$$f_{MC} = \left(\frac{\sigma_{22}}{2S_{21}}\right)^2 + \left(\left(\frac{F_{2c}}{2S_{21}}\right)^2 - 1\right)\frac{\sigma_{22}}{F_{2c}} + \left(\frac{\tau_{12}}{S_{12}}\right)^2 \tag{7}$$

in which f_{FT} is the fiber tension failure index, f_{FC} is the fiber compression failure index, f_{MT} is the matrix tension failure index, and f_{MC} is the matrix compression failure index. The f indices define the initiation of damage mode and range from zero to one, where one indicates that the damage initiation criterion is satisfied. Stress variables are the in-plane longitudinal, σ_{11}, transverse, σ_{22}, and shear, τ_{12}, stress respectively, where the definitions of strength variables are listed in Table 1. A coefficient, α, is used to determine the contribution of the shear stress to the fiber tensile failure, where α is 1 to include the shear stress.

The developed objective function includes three terms for moment performance and one term for the summation of four Hashin indices. Each term in the objective function is defined to obtain a specific operational objective of deployable tube flexures. The objective function is defined as

$$Objective = W_{\mathrm{m}}\Big(\overbrace{\frac{|M_{\mathrm{cte}} - M_{cte}^{target}|}{M_{cte}^{target}}}^{1} + \overbrace{\frac{M_{peak}^{target}}{M_{\mathrm{peak}}}}^{2} + \overbrace{\Big(\frac{M_{peak}^{target} - M_{\mathrm{peak}}}{M_{peak}^{target}}\Big)H(M_{peak}^{target} - M_{\mathrm{peak}})}^{3}\Big) + W_{\mathrm{h}}\overbrace{\Sigma HSN_{\mathrm{all\ modes}}}^{4} \tag{8}$$

1. The first term requires that the constant bending moment be equal to $M_{\mathrm{cte}}^{\mathrm{target}}$. For any design that M_{cte} is greater or less than the target value, the design will be penalized by the value of $\frac{|M_{\mathrm{cte}} - M_{cte}^{target}|}{M_{cte}^{target}}$.
2. The second term is a fraction of M_{peak}^{target} to M_{peak} which aims to maximize the peak moment as high with respect to the M_{peak}^{target}.
3. The third term requires that the peak moment be equal to or greater than the M_{peak}^{target}. For any design for which M_{peak} is less than the target, the design will be penalized by the positive value of $\frac{M_{peak}^{target} - M_{\mathrm{peak}}}{M_{peak}^{target}}$. The Heaviside step function, H, is included to emphasize those designs for which M_{peak} is greater than the target. When M_{peak} is greater than the target, H is switched to zero. On the other hand, for those designs for which M_{peak} is less than the target, H is switched to one.
4. The last term is a summation of Hashin failure indices as discussed in Eqs. (4)–(7).

The factors W_{m} and W_{h} are used as weightings for the moment terms and the Hashin indices term, respectively. In order to demonstrate the general approach, the targets for M_{peak} and M_{cte} are arbitrarily set to be greater than 1700 N·mm and equal to 10 N·mm, respectively, corresponding to 'typical' design values.

In the next section, the optimum cut-outs for rectangle–circle and spline geometries will be presented and a comparison of both optimum schemes will be discussed.

4. Optimization results

In this section, the cut-out shapes obtained from Bayesian optimization are presented for both rectangle–circle and spline parameterizations, where the target moments are greater than 1700 N·mm for $M_{\mathrm{peak}}^{\mathrm{target}}$ and equal to 10 N·mm for $M_{\mathrm{cte}}^{\mathrm{target}}$.

4.1. Rectangle-circle cut-out

The optimized shape for the rectangle–circle cut-out is shown in Fig. 5(a). The moment performance is 1631 N·mm for M_{peak} and 10.2 N·mm for M_{cte}. The stress distribution is shown in Fig. 5(b) and it can be observed that it is highly localized at the circle edges with maximum stress of 627 MPa. This model has no failure and meets with $M_{\mathrm{cte}}^{\mathrm{target}}$ but M_{peak} is lower than the target value of 1700 N·mm. The distribution of primary Hashin indices for matrix and fiber compression (the dominant criteria for this problem) is below one as shown in Figs. 5(c)–5(d) indicating the absence of failure.

4.2. Spline cut-out

Two optimized shapes with highest M_{peak} and no material failure are shown in Figs. 6–7, denoted as the S1 and S2 shapes, respectively. These shapes correspond to optimizations carried out at two levels of

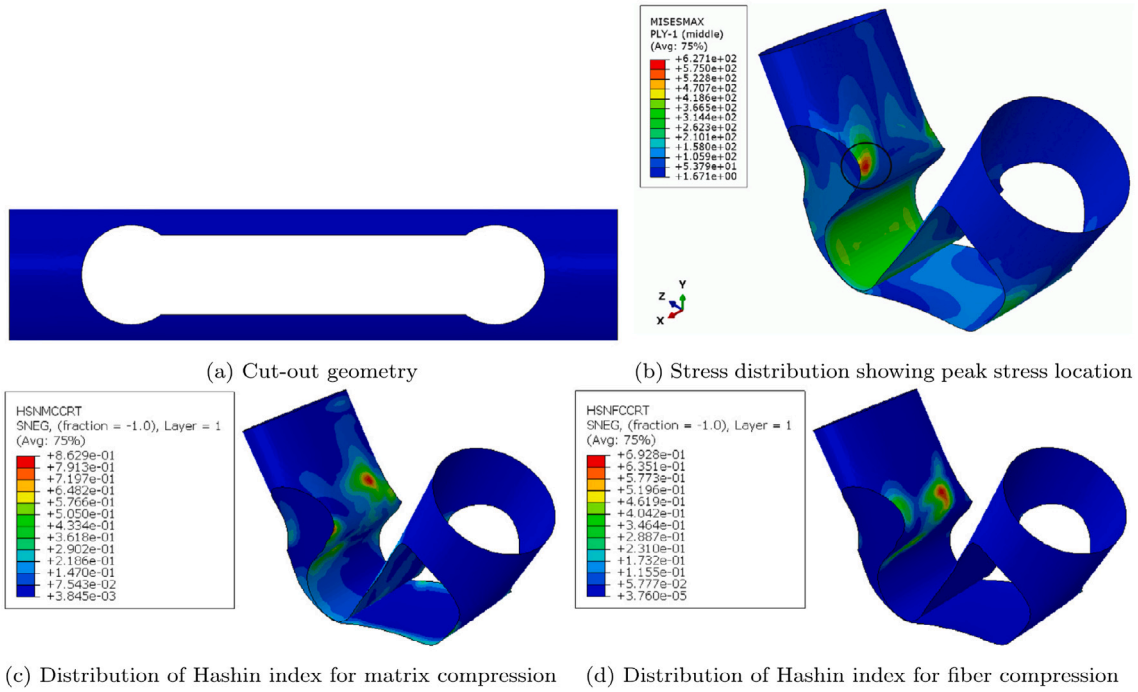

(a) Cut-out geometry (b) Stress distribution showing peak stress location

(c) Distribution of Hashin index for matrix compression (d) Distribution of Hashin index for fiber compression

Fig. 5. Optimized rectangle–circle cut-out geometry.

weighting ratio; the S1 shape is obtained using $W_h/W_m = 1$ and the S2 shape is obtained using $W_h/W_m = 2$, as described in Eq. (8).

The first S1 cut-out shape is shown in Fig. 6(a). Using a spline curve, unlike the rectangle–circle shape, the cut-out shape exhibits a smooth transition which the width gets wider toward the ends of slot and has an almost straight line at the middle of cut-out. It can be observed in Fig. 6(b) that the stress contour is more distributed which the maximum stress is greatly reduced to 480 MPa compared to rectangle–circle cut-out. The distribution of Hashin indices for matrix and fiber compression is presented Figs. 6(c)–6(d).

Finally, the S2 cut-out shape shown in Fig. 7 provides highest M_{peak} among the three optimized shapes. This cut-out shape is similar to the S1 shape with wider ends. The stress contour is also well distributed similarly to the S1 shape while the maximum stresses of the S1 and S2 shapes are comparable. It may be seen that there is no failure indicated in Figs. 7(c)–7(d) corresponding to the dominant Hashin criteria.

In terms of the geometry comparison, it can be seen that the spline parameter allows the cut-out to generate a wide range of shapes and a smooth-transition curve avoiding the localized stress concentration. The S1 and S2 shapes have a similar geometry with the straight line at the middle part of the cut-out and the wider ends, where the wider ends show a more even distribution of stress resulting lower stress value compared with S1 spline and rectangle–circle shapes.

The optimized results for two spline models are summarized in Table 3. The optimum design with regard to maximizing M_{peak} is the S2 shape with 2041 N·mm. These two spline shapes meet with the M_{cte} and M_{peak} target values defined in the objective requirements. The Hashin index for each failure mode is lower than one indicating no failure observed on the tube flexure. However, it should be noticed that the Hashin indices are nearly close to one. The Hashin index of matrix compression failure mode is 0.98 for S1 shape and 0.96 for S2 shape. These optimum designs are close to the onset of failure suggesting the maximum allowable limit of the design. To mitigate against this a margin of safety against material failure can readily be included in the optimization criteria.

During the optimization loop, the regression accuracy for predicting the next candidate point is specified. The absolute error of predicted objective and FE result is calculated in terms of moving average (MA) and plotted in Fig. 8. For the weighting $W_h/W_m = 1$, it can be seen at the very first evolution that the MA of absolute error is high because the regression needs more data points for prediction. After the 6th evolution, MA drops to 10% which means 90% confidence in prediction of the objective function. This means the regression model is well trained and can be used to predict the performance of the tube flexure. Another dashed line of MA for $W_h/W_m = 2$ raises to 33% and then decreases below 10%. However, it should be noted that the identical topography of the S1 and S2 shapes obtained at two levels of weighting confirms a convergence of optimization with a minimal difference in M_{peak}. In both cases, the optimization has been stopped when the MA is less than 10% and the target design values have been achieved without onset of failure.

Table 3
Optimized results for spline parameters regarding M_{peak}^{target} = 1700 N·mm and M_{cte}^{target} = 10 N·mm.

Spline model		S1	S2
Peak moment (N·mm)		1957	2041
Constant moment (N·mm)		10.8	11.4
Hashin indices	Fiber compression	0.92	0.85
	Fiber tension	0.07	0.07
	Matrix compression	0.98	0.96
	Matrix tension	0.86	0.84
Sum of Hashin indices		2.83	2.72

4.3. Optimization summary

To summarize the optimizing process, an optimum cut-out geometry is successfully achieved using Bayesian optimization with both the rectangle–circle and spline-based cut-outs. During the folding simulation, the spline parameters are able to form various cut-out shapes as well as a smooth transition avoiding the highly-localized stress concentration.

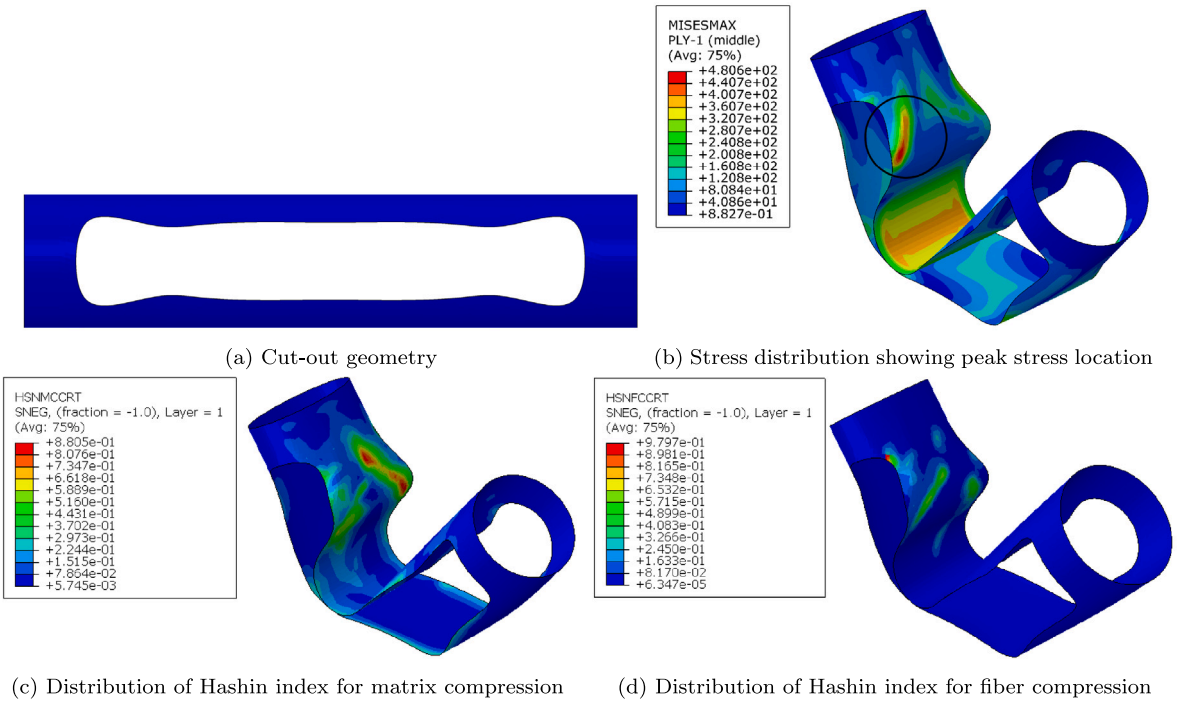

(a) Cut-out geometry (b) Stress distribution showing peak stress location

(c) Distribution of Hashin index for matrix compression (d) Distribution of Hashin index for fiber compression

Fig. 6. S1 shape: optimized spline cut-out geometry for $W_h/W_m = 1$.

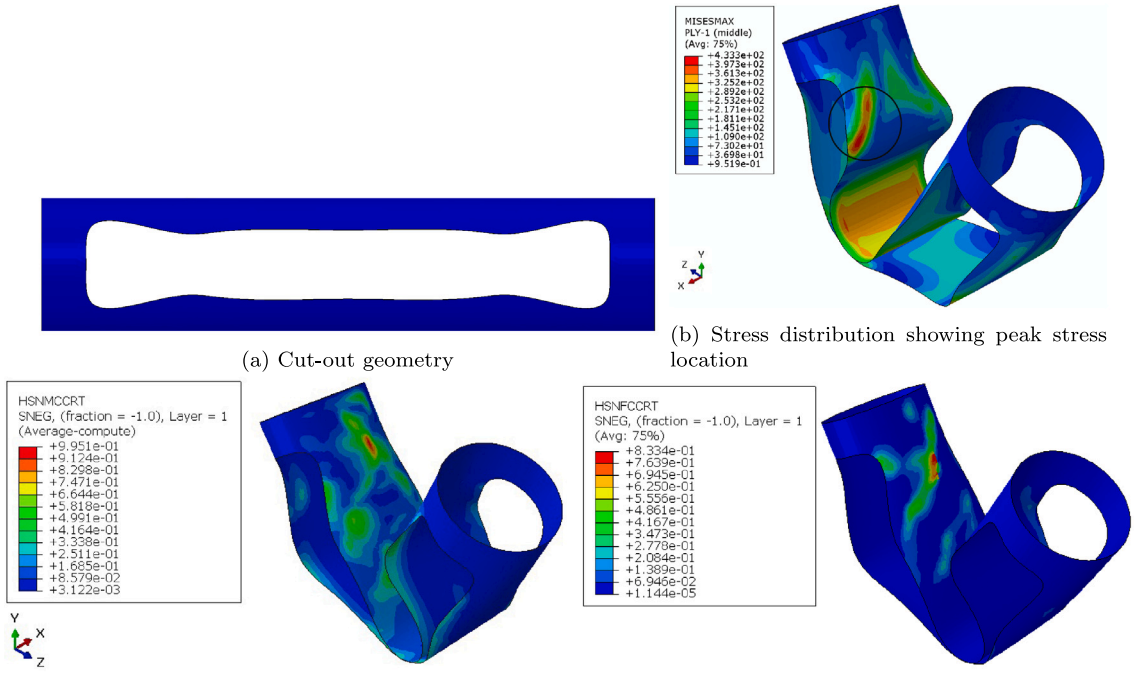

(a) Cut-out geometry (b) Stress distribution showing peak stress location

(c) Distribution of Hashin index for matrix compression (d) Distribution of Hashin index for fiber compression

Fig. 7. S2 shape: optimum spline cut-out geometry for $W_h/W_m = 2$.

The optimized results for rectangle–circle and spline cut-outs are illustrated in Fig. 9 and specific values for the optimum parameters are provided in Table 4. None of the cut-out shapes led to failure of the tube flexures. The most favorable design is located at the upper-left corner of the diagram corresponding to the objective definition of maximizing M_{peak} and minimizing the sum of Hashin indices. As discussed in the previous section, the rectangle–circle parameterization produces a lowest sum of Hashin indices but the targeted M_{peak} of greater than 1700 N·mm cannot be achieved.

The optimized cut-outs, S1 and S2, using spline-based parameterization provide M_{peak} greater than the targeted value while possessing a higher sum of Hashin indices, providing more resistance to folding. Comparing the S1 and S2 shapes, the S2 shape has the highest M_{peak} and also offers a lower sum of Hashin indices. Therefore, the S2 shape is considered as the optimum cut-out design of tube flexure which provides a significant improvement on M_{peak} by 25% compared with the rectangle–circle cut-out.

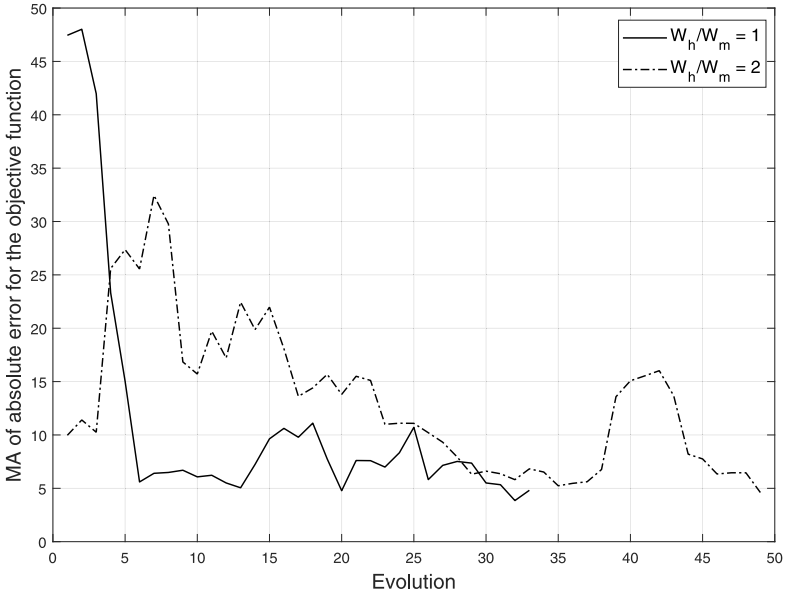

Fig. 8. Moving average of absolute error for objective function for the spline-based optimization.

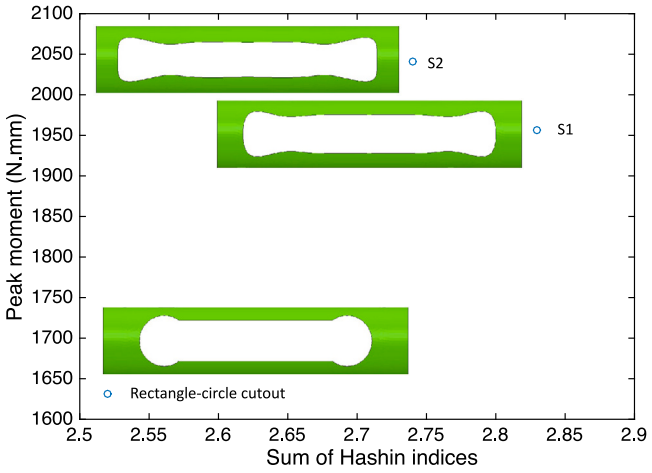

Fig. 9. Summary of spline and conventional cut-out performance.

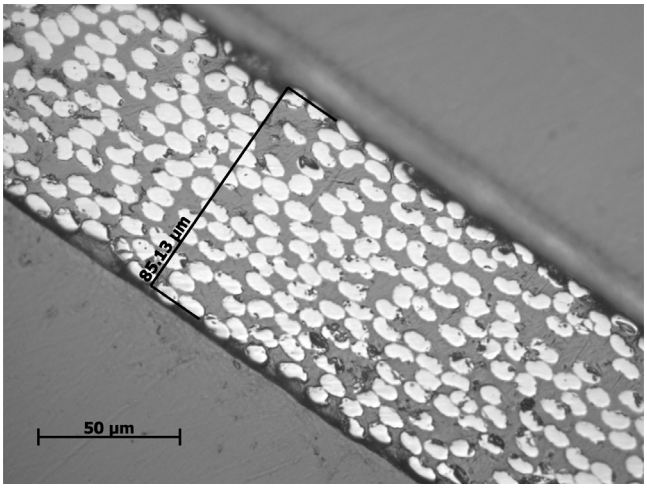

Fig. 10. Example optical micrograph of flexure showing determination of cross section thickness at 50× magnification.

5. Experimental validation

In this section, experimental validation has been carried out to confirm the behavior of the optimum designs achieved from both rectangle–circle and spline cut-out parameterizations. Tube flexures with optimum rectangle–circle and S2 shapes are fabricated and their moment–rotation behavior is determined.

The tube flexures are manufactured with uni-direction pre-preg carbon fibers as given in Section 3.1. The pre-preg plies are laid up by hand on a cylindrical mandrel and cured under vacuum at 125 C° for 90 minutes. The tube thickness is inspected under an optical microscope at a 50× magnification. The thickness is measured at 14 locations with equal spacing on the tube circumference. One such image is shown in Fig. 10. The tube flexure has a mean thickness of 84.8 µm with a standard deviation of 4.2 µm. The consistency of lamina shown in Fig. 10 with the 5% variation for standard deviation indicates that tube flexures are well manufactured. The cut-out shapes are cut using a CNC machine with diamond coated end mills.

The folding experiments have been carried out using the test rig shown in Fig. 11. The tube flexure is attached to the fixed block and another moving block, corresponding to the boundary conditions shown in Fig. 2. The rotations of these blocks are controlled by gear boxes at the base using potentiometers, where the measured rotation has an accuracy of ±0.8° owing to gear backlash. Strain gauges are mounted on hollow shafts connected to each block and are used to covert strain signals to bending moment. The rotation on each side is applied until the moments of two sides are matched indicating that the folding is under a condition of pure bending. This enables meaningful comparison with the finite element simulations.

The experimental results of the optimum rectangle–circle and S2 spline shapes are plotted to compare to the numerical simulations in Fig. 12 where the folding angle is the sum of rotation of both sides of the tube flexure. The simulations are carried out at mean thickness plus and minus one standard deviation. The experimental data show excellent agreement with prediction in terms of M_{peak} values and M_{cte} calculated from average moment between 45° to 135°. For the rectangle–circle cut-out in Fig. 12(a), the M_{peak} and M_{cte} are 1860 and 11.8 N·mm, respectively, while the prediction values at $\bar{t} + \sigma$ are 1960 and 12.5 N·mm, where the differences are 5% and 5.6%, respectively. The spline cut-out in Fig. 12(b) has the M_{peak} of 2588 N·mm above the predicted 2398 N·mm by 8% and M_{cte} is 13.2 N·mm, exactly matching prediction at 13.2 N·mm. The features in the moment response between

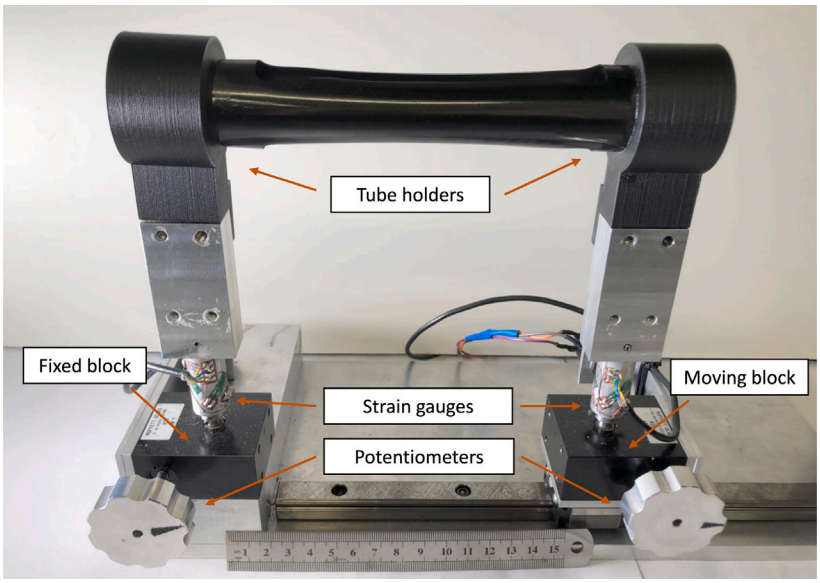

Fig. 11. Experimental rig set-up showing tube flexure, potentiometers, and strain gauges.

Table 4
Optimum cut-out parameters.

(a) Rectangle-circle cut-out	
Parameters	Optimum values
L (mm)	44.69
d (mm)	9.14
r (mm)	−2.72
c (mm)	11.41

(b) Spline cut-outs		
Parameters	Optimum values	
	S1	S2
z_1 (mm)	29.93	29.87
z_2 (mm)	38.75	36.77
z_3 (mm)	55.83	59.24
z_4 (mm)	58.21	59.88
θ_1 (°)	42.4	36.3
θ_2 (°)	38.8	33.8
θ_3 (°)	36.6	31.2
θ_4 (°)	42.7	36.6

Table 5
Comparison of test results and prediction.

Moment performance	Test (N·mm)		Prediction at $\bar{t}+\sigma$ (N·mm)	
	Peak	Constant	Peak	Constant
Rectangle-circle cut-out	1860	11.8	1960	12.5
S2 spline cut-out	2588	13.2	2398	13.2

approximately 90° to 130° correspond to the self contact of the flexure surfaces at this stage of the stowage. These results are summarized in Table 5.

As the experimental results show the key moment performance defined in the optimization objective is achieved and the qualitative comparison between experiment and prediction via simulation shows an excellent agreement with less than 10% error for both peak and constant moments. However, there are two discrepancies that can be noticed in Fig. 12. Firstly the experimental data deviate from the prediction for folding angles above 140°. This deviation is an experimental artifact corresponding to the contact of the exterior surfaces of the test rig. Lastly, the experimental data shows good agreement with the prediction for moments below 500 N·mm but the measured data start to deviate from the prediction for a higher moment. This deviation can be explained by errors associated with the previously-mentioned gear backlash, and additionally uncertainties in the material properties and spatial variations of thickness.

6. Conclusion

This paper has presented a design methodology to investigate the effect of multiple cut-out geometries for deployable tube flexures. A spline-based parameterization is compared to a conventional dog-bone geometry. A Bayesian optimization algorithm is employed to optimize the prescribed cut-out geometries based on desired moment characteristics of the tube flexures in the absence of material failure.

In the optimization process, an objective function has been developed to achieve targeted constant moment while maximizing the peak moment with values specified by the designer, and material failure criteria. The optimization problems are subjected to the objective function with the conventional and proposed spline-based parameterizations. The optimum spline-based geometries achieve the moment targets with the absence of material failure and also show more favorable performance in maximizing the peak moment to 2041 N·mm which is greater than 25% in comparison with conventional cut-out at 1631 N·mm.

Comparing the achievable geometries from the two-considered parameterizations, the proposed spline-based approach is able to form wide-ranging cut-out shapes and smooth transitions within the cut-out geometries. Additionally, it is worth mentioning the benefit of the proposed spline parameterization in terms of stress reduction. The stress is greatly reduced and well-distributed compared with the conventional cut-out, which helps to avoid a localized stress concentration on the cut-out edges. Finally, experimental testing was carried out to verify the moment performance of the optimum cut-out geometries. The experimental results confirm that spline-based parameterization significantly improves the range of achievable performance without onset of failure and also the proposed methodology using Bayesian optimization is effective for designing deployable tube flexures.

By widening the design envelope through the use of improved parameterization schemes and optimization techniques, this work has shown that tube flexures may be designed and fabricated from high-strain composite materials with the ability to tailor for a desired stowage and deployment performance. It is noted that in future work additional design parameters such as the layup may potentially be incorporated to provide further control over the stowage and deployment performance. In conclusion it is hoped that as a result of the

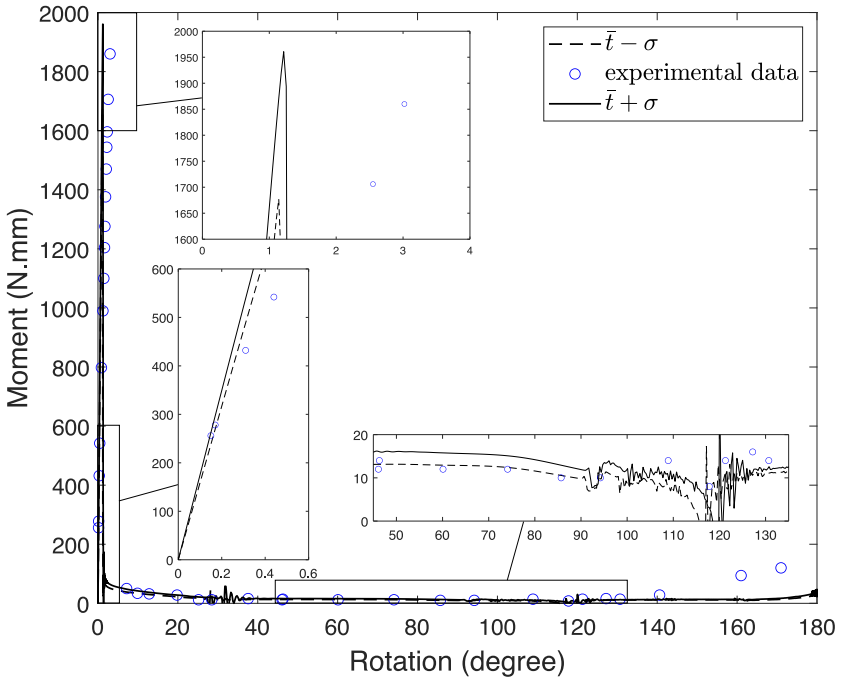

(a) Rectangle-circle cut-out

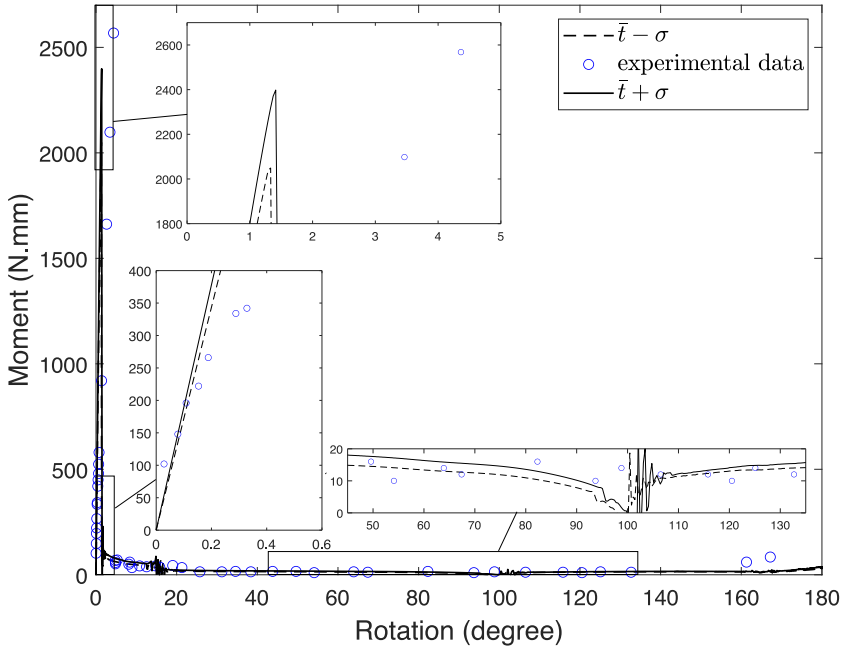

(b) S2 spline cut-out

Fig. 12. Comparison of simulation and experimental results.

increased performance enable through the use of design optimization at the design stage of compliant flexures their usage will continue to grow and enable future novel deployable systems.

Declaration of competing interest

The authors declare that they have no known competing financial interests or personal relationships that could have appeared to influence the work reported in this paper.

Acknowledgments

Pathawee Kunakorn-ong is grateful for financial support from the Royal Thai Government. The authors thank Mr. Jon Cole and Mr. Franco Giammaria for their helpful assistance with the composite manufacture and experimental measurement.

References

[1] K.A. Seffen, S. Pellegrino, Deployment dynamics of tape springs, Proc. R. Soc. A (1999) 1003–1048.
[2] K. Seffen, Z. You, S. Pellegrino, Folding and deployment of curved tape springs, Int. J. Mech. Sci. 42 (2000) 2055–2073.

[3] O. Soykasap, Analysis of tape spring hinges, Int. J. Mech. Sci. 49 (2007) 853–860.
[4] J. Yee, S. Pellegrino, Composite tube hinges, J. Aerosp. Eng. 18 (2005) 224–231.
[5] J. Yee, S. Pellegrino, Folding of woven composite structures, Composites A 36 (2005) 273–278.
[6] H. Mallikarachchi, S. Pellegrino, Quasi-static folding and deployment of ultrathin composite tape-spring hinges, J. Spacecr. Rockets 48 (2011) 187–198.
[7] D. Adams, M. Mobrem, Lenticular jointed Antenna deployment anomaly and resolution onboard the Mars express spacecraft, J. Spacecr. Rockets 46 (2009) 403–410.
[8] L.T. Tan, S. Pellegrino, Thin-shell deployable reflectors with collapsible stiffeners: Part 1 - approach, AIAA J. 44 (2006) 2515–2523.
[9] H. Ye, C. Zhao, Y. Zhang, Q. Yao, Y. Xiao, Analysis of mechanical properties in bending processes and optimal design of simple tape spring, J. Model. Mech. Mater. 1 (2017).
[10] H. Yang, Z. Deng, R. Liu, Y. Wang, H. Guo, Optimizing the qusai-static folding and deploying of thin-walled tube flexure hinges with double slots, Chin. J. Mech. Eng. 27 (2014) 279–286.
[11] H. Mallikarachchi, S. Pellegrino, Optimized designs of composite booms with integral tape-spring hinges, in: AIAA/ASME/AHS Adaptive Structures Conference 12th, 2010.
[12] P.I. Frazier, A tutorial on Bayesian optimization, 2018, arXiv preprint arXiv: 1807.02811.
[13] MATLAB Optimization Toolbox, Matlab machine learning and deep learning toolbox, 2020, The MathWorks, Natick, MA, USA.
[14] SIMULIA, AbaqUS/Explicit, version 2018, 2018, Providence, RI.
[15] Technical data sheet, K51 epoxy pregreg, 2013, http://www.triplehcomposites.co.uk/userfiles/files/SKR20K5120ver1_0(1).pdf. (Accessed 04 January 2021).
[16] R.F. Teixeira, S.T. Pinho, P. Robinson, Thickness-dependence of the translaminar fracture toughness: Experimental study using thin-ply composites, Composites A 90 (2016) 33–44.
[17] Z. Hashin, Failure criteria for unidirectional fiber composites, J. Appl. Mech. 47 (2) (1980) 329–334.